

HIGH-PRECISION ORBIT FITTING AND UNCERTAINTY ANALYSIS OF (486958) 2014 MU69

SIMON B. PORTER,¹ MARC W. BUIE,¹ ALEX H. PARKER,¹ JOHN R. SPENCER,¹ SUSAN BENECHCHI,²
PAOLO TANGA,³ ANNE VERBISER,⁴ J. J. KAVELAARS,⁵ STEPHEN D. J. GWYN,⁵ ELIOT F. YOUNG,¹
H. A. WEAVER,⁶ CATHERINE B. OLKIN,¹ JOEL W. PARKER,¹ AND S. ALAN STERN¹

¹*Southwest Research Institute, 1050 Walnut St. Suite 300, Boulder, CO 80302, USA*

²*Planetary Science Institute, 1700 East Fort Lowell, Suite 106, Tucson, AZ 85719, USA*

³*Université Côte d'Azur, Observatoire de la Côte d'Azur, CNRS, Laboratoire Lagrange, Bd de l'Observatoire, CS 34229, 06304 Nice cedex 4, France*

⁴*University of Virginia, P.O. Box 400325, Charlottesville, VA 22904, USA*

⁵*National Research Council of Canada, Victoria, BC, Canada*

⁶*Johns Hopkins University Applied Physics Laboratory, Laurel, MD, USA*

(Received April 25, 2018; Revised May 2, 2018; Accepted May 3, 2018)

Submitted to AJ

ABSTRACT

NASA's New Horizons spacecraft will conduct a close flyby of the cold classical Kuiper Belt Object (KBO) designated (486958) 2014 MU69 on January 1, 2019. At a heliocentric distance of 44 AU, "MU69" will be the most distant object ever visited by a spacecraft. To enable this flyby, we have developed an extremely high precision orbit fitting and uncertainty processing pipeline, making maximal use of the Hubble Space Telescope's Wide Field Camera 3 (WFC3) and pre-release versions of the ESA Gaia Data Release 2 (DR2) catalog. This pipeline also enabled successful predictions of a stellar occultation by MU69 in July 2017. We describe how we process the WFC3 images to match the Gaia DR2 catalog, extract positional uncertainties for this extremely faint target (typically 140 photons per WFC3 exposure), and translate those uncertainties into probability distribution functions for MU69 at any given time. We also describe how we use these uncertainties to guide New Horizons, plan stellar occultations of MU69, and derive MU69's orbital evolution and long-term stability.

Keywords: astrometry, celestial mechanics, Kuiper belt: general, Kuiper belt objects: individual(2014 MU69), occultations

1. INTRODUCTION

The cold classical Kuiper Belt Object (KBO) (486958) 2014 MU₆₉ is the primary target for NASA’s *New Horizons* Kuiper Belt Extended Mission. The cold classical Kuiper Belt consists of objects on low-eccentricity, low-inclination ($< 5^\circ$ to the invariant plane) orbits (that is, dynamically “cold”) with heliocentric semimajor axes between about 40 and 50 AU. The cold classical objects were likely formed in-place and escaped perturbation from their initial orbits by giant planet migration (Batygin et al. 2011, and references therein), making them the most distant known remnants of the original protoplanetary disk.

NASA’s *New Horizons* spacecraft was launched January 19, 2006, received a gravitational assist from Jupiter on February 28, 2007, and flew through the Pluto-Charon system on July 14, 2015 (Stern et al. 2015). Since the Pluto encounter, *New Horizons* has observed the 3:2 Neptune resonant (15810) Arawn (provisionally designated 1994 JR₁) in 2016 as close at a distance of 0.7 AU (Porter et al. 2016). *New Horizons* will encounter many other KBOs within 1 AU, some as close as 0.1 AU, and some (such as Quaoar and Haumea) that are much farther away, but all can be seen by *New Horizons* at much higher solar phase angles than is possible from Earth-based telescopes (Porter et al. 2018 in preparation, Verbiscer et al. 2018 in preparation). However, none of these KBOs will be seen as close as MU₆₉, which will be within 3500 km of the spacecraft on the nominal trajectory. *New Horizons* will image the surface of MU₆₉ at best resolutions of ≈ 35 meter/pixel, and spectral maps at ≈ 1 km/pixel. In order to guide the spacecraft to such a close encounter with a KBO that only has a relatively short orbital arc required a completely new approach to orbit determination and uncertainty analysis, which we describe in this paper.

2014 MU₆₉ was discovered in July 2014 by the *Hubble Space Telescope* (HST) following eight years of dedicated searches for a second *New Horizons* encounter object (Buie et al. 2018, in preparation). After several ground-based searches down to $V \approx 26$, 194 HST orbits were allocated for a deeper, more systematic search for objects accessible to *New Horizons* (GO 13633, PI Spencer). MU₆₉ was initially detected in 10 images acquired in two HST orbits, as were four other KBOs during the *HST* search. Three objects were potential targets for *New Horizons*: 2014 MU₆₉, 2014 OS₃₉₃, and 2014 PN₇₀. In August 2015, the *New Horizons* team selected 2014 MU₆₉ as the potential *New Horizons* extended mission target. The spacecraft performed a series of four burns in October-November 2015 to target 2014 MU₆₉. The *New Horizons* Kuiper Belt Extended Mission was approved by NASA after Senior Review in July 2016, and its centerpiece is the flyby of 2014 MU₆₉ on January 1, 2019.

In this paper, we will discuss our process of performing absolute astrometry on 2014 MU₆₉ tied to a pre-release version of *Gaia* DR2, propagating that error forward to orbital uncertainty, and then using the orbital uncertainty to guide both occultations of the KBO and to guide the spacecraft to a close flyby. These techniques represent the highest-precision heliocentric orbit fitting of a Kuiper Belt object ever, and can provide a basis for future applications of *Gaia*-driven astrometry to small bodies in the solar system.

2. DATA SOURCES

2014 MU₆₉ was discovered with the *HST* search program (GO 13633) described in (Buie et al. 2018, in preparation). This program was designed to take five full-frame 370-second Wide Field Camera 3 (WFC3) UVIS images in one orbit with the F350LP broadband filter, skip an *HST* orbit, and then repeat the same observation. The images were tracked on a

nominal cold-classical orbit, producing streaked stars, but non-streaked KBOs. To perform the search, the images were shift-stacked at 20 different representative cold-classical shift rates. Objects that appeared in both search orbits for one of the shift rates were identified and targeted for follow up *HST* observations. The first object identified this way was designated 1110113Y (HST orbit IDs 11/12, WFC3 CCD 1, shift rate ID 011, random ID 3Y), later given the provisional designation 2014 MU₆₉. Four more KBOs were subsequently detected, all of which were brighter, but all of which required more fuel for *New Horizons* to reach.

The available dataset for 2014 MU₆₉ has both a short temporal arc (July 2014-October 2017), and an extremely high data quality, making it ideal for the analysis described below. MU₆₉ is a very faint object, with $V \approx 27.5$ (Benecchi et al. 2018, in preparation), and is in an extremely crowded star field (galactic longitudes from -8° to -12°). These constraints have made it effectively impossible to detect with ground-based telescopes, and all observations of MU₆₉ have been with the *Hubble Space Telescope*. A list of these *HST* observations is in Table 3.

Both the initial follow up observations and most observations conducted since then have adopted the search program’s basic format of five 367 to 370-second, F350LP filter, full frame UVIS WFC3 images. The key exceptions are the color campaign in summer of 2016 (GO 14092, PI Benecchi), in which four orbits each included two 348-second images using F606W followed by three 373-second images with F814W. As shown in Table 3, half of the follow up orbits were roughly evenly spread over August 2014-October 2017, while the other half were spread over a roughly one week interval in June-July 2017. The latter was the lightcurve campaign (GO 14627, PI Benecchi), which was critical in successfully predicting the July 2017 occultation (See Section 6).

In addition to *HST* and the July 2017 occultation, the other data source for this analysis was stellar astrometry from the ESA *Gaia* project. Initially, the process in Section 3 was built using a custom star catalog built from a deep composite of the MU₆₉ field obtained using the Canada-France-Hawaii Telescope (Gwyn 2014). When the *Gaia* Data Release 1 (DR1) was made available in September 2016 (Gaia Collaboration et al. 2016), we began using that, applying a mean proper motion correction to images significantly after the DR1 2015.0 epoch. The mean proper motion was calculated from the *Gaia* TGAS catalog (Michalik et al. 2015). The MU₆₉ observation fields were in areas of very low coverage for TGAS, so the TGAS stars could not be used directly. With the success of our application of DR1 and after a special support request to the *Gaia* project, we were able to obtain a sky patch from a pre-release version of Data Release 2 (DR2) around the path of MU₆₉. The major advances with DR2 are proper motion for all catalog stars, obviating the need for a mean proper motion correction, as well as a much more homogeneous, bias-free distribution of errors on the sky, and much lower uncertainty (one order of magnitude). This early version of DR2 was used to plan the three 2017 occultations, both for correcting the *HST* absolute astrometry and for knowledge of the occultation stars themselves. We obtained a second preview version of DR2 in our field of interest in October 2017, and that version is used for the astrometry in Table 3.

3. IMAGE ANALYSIS

A typical *HST* MU₆₉ image is shown in Figure 1. Over the course of 2014-2017, MU₆₉ has moved between galactic latitudes of -8° and -12° . Accordingly, the background star density has always been very high in any images of MU₆₉ (from both Earth and *New Horizons*), and this dense background field will persist through the *New Horizons* encounter. To mit-

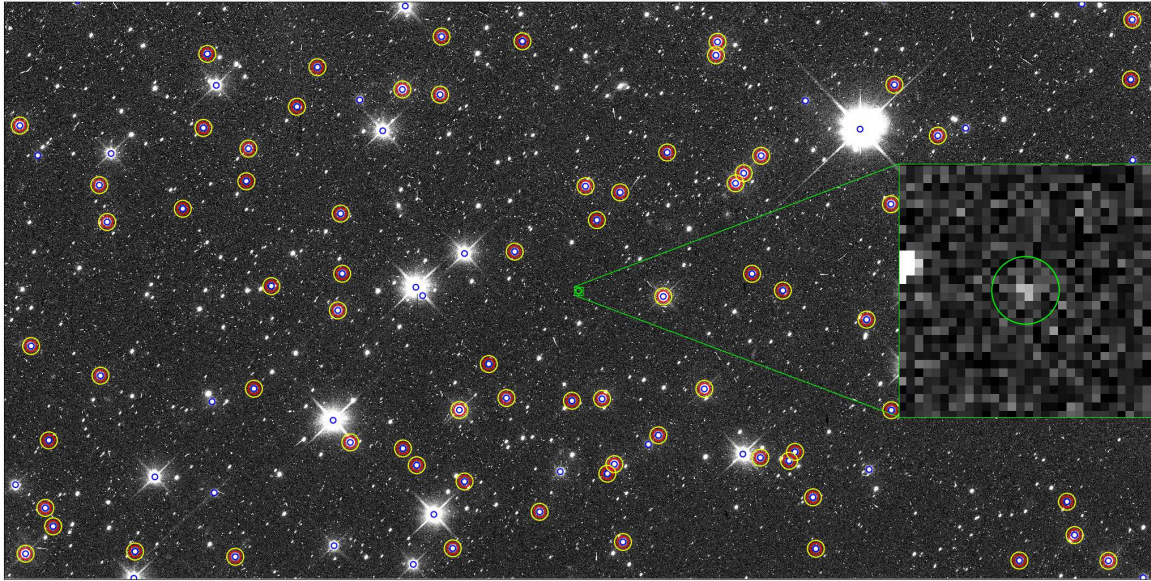


Figure 1. An image from the HST lightcurve campaign (id8i16moq). The blue circles show the *Gaia* DR2 positions of stars, the red circles show the locations of star PDFs used for the WCS solution, and the outer yellow circles indicate a match (all PDF stars were matched in this case, which is typical). The inset green box shows the location of 2014 MU₆₉; see Figure 2.

igate this background, we developed a Python program called *warpy.py* to perform simple star subtraction. Because almost every observation sequence consists of five images of roughly the same field, *warpy.py* iterates through the images, warps the other four images of the visit to the frame of the fifth, median combines the four warped images, and subtracts them from the target image. The images are coregistered by matching sources detected with *Source Extractor* (Bertin & Arnouts 1996). Because the stars in the images are all smeared differently, they do not subtract cleanly. However, the star-subtracted images are useful for verification that the following steps are fitting the KBO and not a background source.

The smeared stars are also a problem for determining the pointing of the images. Since *HST* is tracking on the motion of the object, a single Tiny Tim (Krist et al. 2011) point spread function (PSF) would not accurately describe the effective PSFs of the stars. We thus built up “smear kernels” that describe the motion of the stars relative to the KBO through the 370

second exposures. By shifting a Tiny Tim PSF to 400 discrete times during the exposure and averaging them, we were able to build up an exact model of each star’s PSF. We did this for each star used for the WCS solution (effectively, all the *Gaia* stars in the field), since the Tiny Tim PSF varies across the WFC3 field.

We next used the stellar PSFs to build up probability distribution functions (PDFs) for the pixel location of each star within each image. We did this task with a Markov-Chain Monte Carlo (MCMC) algorithm implemented in IDL. This minimal MCMC with a single “walker” was iterated for 2000 steps to build a PDF of both pixel position and total DN/second flux. The result is 2000 equal-probability pixel positions for the star, encompassing the true shape of the uncertainty distribution. We found this number of steps to be sufficient, as all the stars used in the astrometric solution had a high signal-to-noise ratio and typically there were 70-100 stars used in a given solution. The flux number was not used directly in the fits, but provided diagnostics if the fits

were successful. A typical star had a $1\text{-}\sigma$ pixel position uncertainty of <0.1 pixels, equating to an angular uncertainty of <4 milliarcseconds.

With these stellar PDFs, we could now build PDFs for the pointing of *HST* in each image. WFC3 UVIS images use a three-layer World Coordinate System (WCS) to translate pixel to sky coordinates, as described in Greisen et al. (2006). The first layer is the basic pointing, roll, and trapezoidal warp, the second is a set of SIP polynomials that describe the low-frequency distortion on the chip, and the third layer is a look-up table that describes high-frequency pixel distortion (e.g. by irregularities in the lithography of the CCD). All of the distortion parameters are highly-calibrated, and we only needed to update the pointing with deltas to the *CRVAL1* and *CRVAL2* keywords, and the roll by multiplying the CD matrix by a rotation matrix. Thus for each image we have three parameters for the WCS PDF: delta RA, delta Dec, and delta roll. We built this WCS PDF by selecting a pixel coordinate for each star from their PDFs, fitting a best-fit WCS solution, and recording the deltas from the original WCS. This process was repeated 10,000 times to build a discretely-sampled PDF of the WCS offsets. The resulting typical $1\text{-}\sigma$ uncertainty in the *CRVAL1* and *CRVAL2* keywords (and thus in the pointing of *HST*) was <2 milliarcseconds.

The pixel position PDFs for the KBO used the same basic MCMC algorithm as the star pixel PDFs, but with the single walker iterated 10000 times to build the PDF. Since *HST* tracked on the KBO, we did not need a smear kernel to fit the KBO and could use a Tiny Tim PSF directly. In addition, all but the discovery observations had MU₆₉ near the center of WFC3 chip 2 (FITS extension 1), making for a less distorted PSF than near the chip edges. Initially, the KBO fit was started with a manual click on the rough position of the KBO in the image. However, as the orbit improved, this manual po-

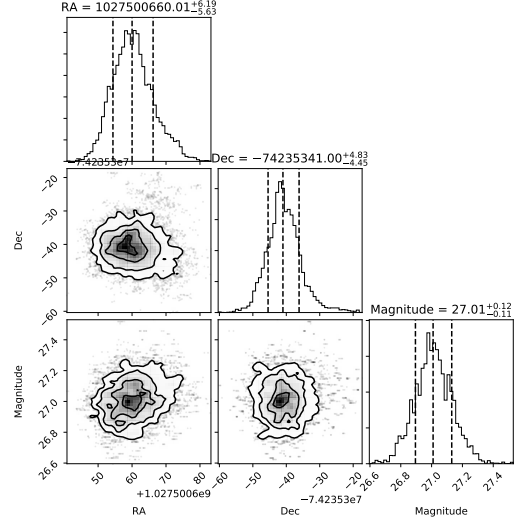


Figure 2. The RA/Dec/Magnitude Probability Distribution Function (PDF) for MU₆₉ in the image id8i16moq (see Figure 1). RA and Dec are in milliarcseconds, so as to show the uncertainty in appropriate units. We generated similar PDFs for all the astrometry shown in Table 3.

sition was replaced with a calculated initial position from prior orbit solutions and the WCS. We also made manual masks of stars and cosmic rays near the KBO that might adversely affect the PDF generation.

Finally, we needed to combine the KBO pixel PDFs with the WCS PDFs to make KBO sky PDFs. Similarly to the WCS PDFs, this was accomplished by selecting a randomly-selected KBO pixel location with a randomly-selected WCS PDF, translating to RA and Dec, and then repeating 10,000 times. An example of one of these PDFs is shown in Figure 2. The instrument magnitude in the pixel PDF was converted to AB apparent magnitude with the PHOTFLAM header keyword. While the magnitude was not used directly for astrometry, it was an important diagnostic for the quality of the pixel PDF. For the solutions presented, we filtered out any points with magnitude uncertainties larger than 0.5, which were generally failures to fit the object, or any points with uncertainties smaller than 0.1 magnitudes, typi-

cally a cosmic ray close to the KBO causing spuriously high signal-to-noise ratios. We also only used the F350LP points for the orbit, as the narrower-band points had worse signal-to-noise ratios for both stars and MU₆₉. This left 214 of the 264 images, which we used for an initial fit. An additional nine points were rejected because they had greater than 30 milliarcsecond residuals relative to the initial fit. Our final HST astrometry thus used 205 of the 264 images (78%); these are shown in Table 3.

After the method described here was used to successfully predict the occultation of MU₆₉ on July 17, 2017 (See Section 6, Buie et al. 2018, in preparation), we were able to use the occultation itself as a high-quality occultation point. Because five solid-body chords were obtained on July 17, we chose the mid-time of the longest chord and used it as the nominal center-of-figure. We could then combine this mid-time, the topocentric location of the portable telescope that obtained the longest chord, and the location and uncertainty of the occultation star from *Gaia* DR2 to produce an effective astrometric PDF. See Buie et al. (2018, in preparation) for more details about the circumstances and analysis of this occultation. This occultation PDF could then be combined with the *HST*-derived PDFs in the process described in Section 4.

4. ORBIT DETERMINATION

Typically, small body orbits in the literature are described in either mean or osculating heliocentric elements, with error bars representing a normal error distribution. This is typically sufficient for general dynamical studies and rough targeting from the ground, but not for spacecraft flybys or occultation planning. The actual uncertainty of an object’s astrometry is rarely perfectly described by a normal distribution, and neither is that object’s location and velocity in space. We thus sought to develop an orbit-fitting method that would accurately

map the full astrometric uncertainty distribution into the ephemeris.

To perform these fits, we developed a high-precision few-body orbital integrator. Since 2014 MU₆₉ is a cold-classical KBO, all of the planetary perturbations on it are interior, and tend to result in a slow precession. Non-gravitational factors (i.e. YORP) and general relativity are not a factor for Kuiper Belt objects. We therefore developed a few-body conservative force integrator, capable of modeling the major planets and their perturbing forces on a massless test particle. This integrator (PyNBody¹) is based on the 12/13th order Runge-Kutta-Nystrom integrator of Brankin et al. (1989) and was previously described in Porter et al. (2016). This integrator is not the fastest, but it is very accurate and can typically conserve system energy and momentum to within machine precision over the relevant timescales for orbit fitting.

The KBO’s orbit is parameterized as a cartesian state vector relative to the solar system barycenter at a fixed epoch. The inertial frame for the integrations the International Celestial Reference Frame (ICRF). *Gaia* DR1 is aligned to ICRF by matching optical detections of quasars with a subset of ICRF2, while *Gaia* DR2 uses several thousand quasars from ICRF3 and half a million AGNs to perform frame alignment (Gaia Collaboration et al. 2016). The integration epoch is set to 2014-06-01 00:00:00.000 UTC, a few weeks before the first observation (originally a safety factor in case of any precoversies in the *HST* search). To test the solution against the data, we propagate the state vector with the PyNBody integrator to the desired time and calculate its apparent ICRF RA/Dec from *HST*, with appropriate light-time correction. We use the JPL NAIF *HST* and *DE430* SPICE kernels to determine the location of *HST*

¹ <https://github.com/ascendingnode/PyNBody>

relative to the solar system barycenter (Folkner et al. 2014).

We used the *emcee* Markov-Chain Monte Carlo package (Foreman-Mackey et al. 2013) to translate the astrometric uncertainty to orbital uncertainty. The *emcee* package provides a fast and natively multithreaded way to run MCMC from Python. As input to *emcee*, the fitting program calculates the likelihood for any solution by taking the predicted RA/Decs for that solution and comparing them to the RA/Dec PDFs. Because the PDFs are discretely-sampled, we created a Kernel Density Estimator (KDE) for each observations, using Silverman’s Rule of Thumb (Silverman 1986) to choose the bandwidths, since most of the PDFs were roughly Gaussian. The log likelihoods for all the images could then be summed to provide a total log likelihood to *emcee*.

For any solution, the first step is to make an initial guess (typically an older solution) and minimize its χ^2 with a downhill simplex method (Nelder & Mead 1965). This polished solution is then used to create 200 slightly perturbed state vectors as the initial “walkers” for *emcee* to use. We then run the 200 walkers for 100 iterations to “burn-in” and allow them to move away from the artificial initial distribution. We then reset *emcee* and run it for 500 iterations to produce the full PDF cloud of 10,000 state vectors at the fitting epoch. These numbers of iterations were arrived at after much testing, and are typically more burn-in than is actually necessary, so as to ensure that the solutions are well-distributed. We save the resulting state vector PDF in a format that can then be propagated to any time of interest. The state vector and orbit for our “rd2b” orbit solution are presented in Table 1

While the full PDF cloud of 10,000 states encapsulates the uncertainty in the location of MU₆₉ any any time, it is rather unwieldy to use in most circumstances. We therefore calculated the state clouds of 2014 MU₆₉ at 2000 discrete

Table 1. The “rd2b” orbit solution for 2014 MU₆₉. State vector and orbit are relative to the solar system barycenter and in the ICRF Ecliptic frame at the epoch 2014-06-01 00:00:00 UTC.

	Value		1- σ	
x	+1.163133074444e + 09	±	2.80233e + 02	km
y	−6.385039581373e + 09	±	1.52754e + 03	km
z	+2.373261916929e + 08	±	5.87015e + 01	km
v_x	+4.461378977476e + 00	±	5.92714e − 06	km/s
v_y	+9.619622770583e − 01	±	2.45488e − 05	km/s
v_z	−1.066958207821e − 01	±	9.45150e − 07	km/s
a	44.23555350	±	0.00003999	AU
e	0.03787388	±	0.00000476	
I	2.44993086	±	0.00000203	deg
Ω	159.04712465	±	0.00006746	deg
ω	183.74800591	±	0.00469779	deg
M	301.30454775	±	0.00406885	deg

times between January 1, 2004 and January 1, 2024, and averaged the states at each time. We then generated order-27 Chebyshev polynomials (Tchebychev 1853) for the positions of the KBO, and saved them in a JPL SPICE Type 02 SPK kernel. JPL SPICE could then be used to rapidly interpolate the location of MU₆₉ at any time along the interval. Testing the kernel at 769 random points over the interval returned a root-mean-squared residual of 20 meters, well below the uncertainty in the orbit.

5. NEW HORIZONS TRAJECTORY PLANNING

The primary reason to determine the orbit of 2014 MU₆₉ to very high precision is to ensure the success of the *New Horizons* flyby. *New Horizons* performed the major Trajectory Correction Maneuver (TCM) to guide it to MU₆₉ over a series of four burn segments in October

and November 2015, after all Pluto observations had finished. The initial orbit used to target the spacecraft was based on the first year of data, from June 2014 to July 2015 (GO 13633 and GO/DD 14053, PI Spencer). After that burn, early versions of the analysis described here showed that significantly more *HST* observations would be required to enable a close flyby of 2014 MU₆₉. We thus proposed and were awarded six *HST* orbits in 2016, and five in 2017 (GO/DD 14485, GO 14629, and GO 15158, PI Buie). In addition, 24 *HST* orbits were used in June/July 2017 to measure the lightcurve of MU₆₉ (GO 14627, PI Benecchi). The orbit presented here uses data from all of these *HST* programs, in addition to the July 17 occultation.

The *New Horizons* spacecraft will nominally fly closest to 2014 MU₆₉ at 05:33 January 1, 2019 UTC. This time was chosen to enable both the Goldstone and Canberra Deep Space Network (DSN) 70-meter dishes to uplink to the spacecraft simultaneously for an attempted bistatic radar experiment (as was performed at Pluto; [Linscott et al. 2016](#)). *New Horizons* will not be able to acquire MU₆₉ any earlier than August 2018. Because of *New Horizons*'s almost radial trajectory out of the solar system, the KBO will move very slowly against the background stars until a just few weeks before encounter. While the spacecraft can use the Long Range Reconnaissance Imager (LORRI, [Conard et al. 2005](#)) to well constrain the location of 2014 MU₆₉ in the “B-Plane” (the plane perpendicular to the spacecraft’s motion and containing the flyby target), the time-of-flight (ToF) uncertainty along the direction of the spacecraft’s motion is constrained only by the Earth-based orbital solution. The distance to the spacecraft from Earth will be well-constrained by Doppler radio measurements on approach to MU₆₉, and so the uncertainty in the absolute location of MU₆₉ relative to the solar system barycenter will determine the flyby ToF uncertainty.

6. APPLICATION TO OCCULTATION PLANNING

In addition to guiding *New Horizons*, we also used our orbit solution to predict three stellar occultations by 2014 MU₆₉ in 2017 and one in 2018. The 2017 occultation campaign is comprehensively described in [Buie et al. \(2018, in preparation\)](#) and here we detail only the procedures used to predict the occultations. MU₆₉ is a small object, with an absolute magnitude of $H_V \approx 11$ [Benecchi et al. \(2018, in preparation\)](#), corresponding to a size likely smaller than 50 km diameter. We therefore knew that the occultations would only be successful if we had very high-quality orbital estimates and uncertainty models. Thankfully, that is exactly what we had developed for guiding *New Horizons*.

Stellar occultations occur when a solar system object passes in front of a star from the perspective of an observer. They have been used to discover the atmosphere of Pluto ([Elliot et al. 1989](#)) and the rings around Uranus, Chariklo, and Haumea ([Elliot et al. 1977](#); [Braga-Ribas et al. 2014](#); [Ortiz et al. 2017](#), respectively). The latter is most important for planning the *New Horizons* flyby of MU₆₉, as occultations provide the only way of detecting rings or other opacity structures around the KBO before the spacecraft is close enough to see them directly. In addition, occultations can (and in this case did) provide estimates of the size and shape of a body. Knowledge of the approximate size of MU₆₉ enabled estimates of its bulk albedo, and therefore allowed mission planners to better estimate the correct exposure times for the flyby images.

Because of the motion and rotation of the Earth, stellar occultations sweep across Earth from west to east. The typical approach to observe an occultation of an object with an uncertain orbit is therefore to set up a north-south “picket fence” of portable telescope teams perpendicular or “crosstrack” to the occultation

path. It is therefore important to know both the crosstrack uncertainty of the prediction, and what the crosstrack distance of any station is. The latter often requires some iteration, as finding a logistically viable site with the proper crosstrack can be challenging, especially in an unfamiliar country. We thus developed tools to export KML files to Google Maps with lines showing the target crosstracks for each observing team. These could be used for planning site reconnaissance, and with GPS-enabled smartphones, used to see in real time where a potential site was located compared to the desired crosstrack line. To estimate the crosstrack uncertainty, we propagated the full 10,000 states to the occultation time and calculated the geometry for all of those states. This produced a full PDF of the occultation uncertainty, which we could use to plan the crosstracks to maximize the chance of success.

The first MU₆₉ occultation of 2017 was on June 3. The ground track for this event passed over both South America and South Africa, and 25 portable telescope teams were deployed to both Mendoza, Argentina and the Northern Cape and Western Cape Provinces of South Africa. Two *HST* astrometric observations of MU₆₉ had been planned for the spring of 2017, on March 16 and in mid May. However, the March observation failed due to a safing event on *HST*, and the observation could not be rescheduled in April, because MU₆₉ was passing through quadrature and did not have enough sky motion from *HST* to be detected. Thus, the first MU₆₉ observations of 2017 were acquired by *HST* on May 1 and 25. An initial solution though May 1, “may1c”, was used to plan the deployments to Argentina and South Africa. This was superseded by the “may25a” solution with data through May 25, which was produced after the orbit fitters (Porter and Buie) had deployed, and was used to plan the actual ground tracks. The “may25a” solution purported to

Table 2. Mean, Free and Forced Elements for Best-Fit MU₆₉.

Best Fit,	10 ⁸ years
Mean a	44.23 AU
Forced e	6×10^{-5}
Free e	0.037
Forced i_{mss}	0.26°
Forced i_{mkb}	0.0012°
Free i	2.54°

have a crosstrack uncertainty of 44 km, though the subsequent June-July 2017 observations showed that the “may25a” ground track had been too far north by almost 2-sigma. This offset precluded a solid-body occultation on June 3, though the high signal-to-noise ratio observations of the event at the South African Astronomical Observatory 74-inch telescope and at Gemini South did exclude optically-thick rings around MU₆₉. See Buie et al. (2018, in preparation) for more details.

The second MU₆₉ occultation of 2017 was on July 10. This event occurred mainly over the Pacific Ocean with a much dimmer star ($V \approx 15.5$) and nearly-full Moon, thus preventing a ground-based observation campaign. However, the NASA-DLR Stratospheric Observatory for Infrared Astronomy (SOFIA) airborne observatory was able to reach the occultation track from its southern deployment base in Christchurch, New Zealand, and NASA awarded a flight to observe the July 10 occultation (PI E. Young). Between the June 3 and July 10 events, *HST* observed 2014 MU₆₉ over 24 orbits between June 25 and July 4 (GO 14627, PI Benecchi). This program provided a wealth of new images to integrate into the MU₆₉ orbit solution in a very short amount of

time, and time was especially critical, as the last six orbits worth of data was downlinked from *HST* after the orbit fitting team (Porter and Buie) had arrived in Christchurch. Thus, the orbit solution used to guide the SOFIA flight was necessarily determined at the United States Antarctic Program Christchurch facility, and delivered to the SOFIA mission planners 36 hours before the flight. This orbit solution, “lc1”, used all of the lightcurve campaign points, plus the highest-quality preceding *HST* MU₆₉ observations.

The final MU₆₉ occultation of 2017 on July 17 was observed with portable ground stations in the Chubut and Santa Cruz provinces in Argentina. No additional observations of *HST* MU₆₉ were made between the July 10 and July 17 occultations, but we did perform a more thorough filtering of low-quality points. This resulted in the “lc1gr” solution that was used to guide the placement of stations for the July 17 occultation. The “lc1gr” solution had a $1\text{-}\sigma$ uncertainty in crosstrack of 13 km, much tighter than for June 3. This solution allowed a tighter picket fence of stations up and down the Patagonian coast, centered a few kilometers north of the city of Comodoro Rivadavia. Despite high winds on the occultation night, 22 of the 24 deployed stations successfully observed the occultation. Five of those stations observed the solid-body occultation, with the southernmost being the predicted centerline from the “lc1gr” solution.

This work predicts an additional stellar occultation opportunity on August 4, 2018. The ground track for this event passes over western Africa (Mali, Mauritania, and Senegal) and northern South America (Guyana, Venezuela, and Colombia). With the “rd2b” solution presented in Table 1, the $1\text{-}\sigma$ crosstrack uncertainty is 12 km. This uncertainty will decrease somewhat with additional *HST* observations in 2018.

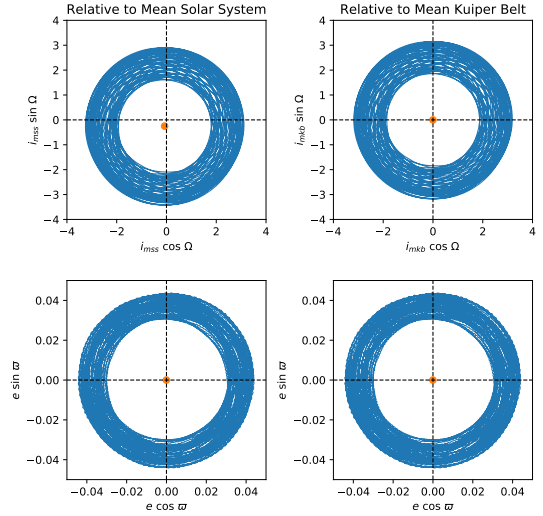


Figure 3. Free and forced elements for best-fit 2014 MU₆₉; the centers of the circles show forced inclination/eccentricity, while the radii show free inclination/eccentricity. The forced inclination is 0.26° from the mean solar system angular momentum vector (left), but almost perfectly fits the mean Kuiper Belt at 44 AU pole from Volk & Malhotra (2017, right). The lack of forced eccentricity or inclination implies that MU₆₉ has not experienced any significant orbital evolution since formation.

7. LONG-TERM ORBITAL EVOLUTION

2014 MU₆₉ is a cold classical Kuiper Belt object. Elliot et al. (2005) identified the “Classical” KBOs as non-resonant objects with eccentricities smaller than 0.2. This classification was further refined as a “Cold Classical” or “Kernel” population by Petit et al. (2011) with $a \approx 44$ AU, $e \approx 0.05$, $i < 5^\circ$ to the invariant plane. MU₆₉ has $a=44.2$ AU, $e=0.03$, $i=2.4^\circ$, making it an archetype of the cold classical population. Batygin et al. (2011) showed the orbits of cold classical objects were likely formed in-place and survived being disturbed from their initial orbits by giant planet migration. The unusually high binary fraction of cold classical KBOs (Noll et al. 2008) is an additional line of evidence that they are mostly undisturbed from their original orbits. Indeed, the observed cold classical KBO binary fraction is high enough that

nearly all must have originally formed as binaries or higher-order multiple systems (Fraser et al. 2017).

With a few small modifications to the PyN-Body code, we were able to integrate the orbit of MU₆₉ over sufficiently long timescales to test this stability and determine mean orbital elements. Specifically, we changed the time unit in the integration from seconds to years to allow for longer integrations without worry of overflows and removed the terrestrial planets as perturbers (instead dropping their masses into the Sun). The results of integrations forward and back 10⁸ years can be seen in Figure 3 and Table 2, projected in both the mean solar system plane defined by the *de430.bsp* planets in the ICRF J2000 Ecliptic frame, $i_m = 1.6^\circ$ and $\Omega_m = 72.4^\circ$, and in the mean Kuiper Belt plane at 44 AU as determined from known KBOs Volk & Malhotra (2017), $i_m = 1.8^\circ$ and $\Omega_m = 77.0^\circ$. The mean, free, and forced elements of MU₆₉'s orbit are shown in Table 2. The forced inclination of MU₆₉ to the mean solar system plane is 0.26°, but only 0.0012° to the mean Kuiper Belt at 44 AU. Likewise, the forced eccentricity of MU₆₉ is less than 0.0001. The apparent lack of any forced inclination or eccentricity to the mean Kuiper Belt is strong evidence that MU₆₉ has not suffered any significant orbital evolution beyond secular perturbations. MU₆₉ should therefore represent a truly pristine fossil of the Sun's protoplanetary disk, an object unlike any other previously visited by a spacecraft.

8. SUMMARY

We have described the process we have used to fit the orbit of 2014 MU₆₉, as of the start of 2018. This process combines *Gaia* DR2 and *HST*/WFC3 to produce extremely high precision absolute astrometry of MU₆₉, and trans-

lates that uncertainty into a cartesian state vector probability distribution function that can be evolved to any time of interest. The results of this analysis were used to successfully predict and observe a solid-body stellar occultation of MU₆₉ on July 17, 2017, predict a stellar occultation on August 4, 2018, and to guide the *New Horizons* spacecraft to a close (3500 km) flyby of MU₆₉ on January 1, 2019.

The process described here should enable high-precision orbit determination for future occultations and spacecraft missions. 2014 MU₆₉ presents the extreme case of a very interesting object that is both faint and in a very crowded star field. Now that the *Gaia* DR2 catalog has been released, solar system objects with higher signal-to-noise ratios should benefit even more from this technique, enabling a substantial improvement in orbital uncertainty and increasing the number of objects that might be observed with stellar occultations.

This work was supported by NASA's *New Horizons* mission and *HST* programs GO 13633, GO/DD 14053, GO 14092, GO/DD 14485, GO 14627, GO 14629, and GO 15158. Support for this program was provided by NASA through a grant from the Space Telescope Science Institute, which is operated by the Association of Universities for Research in Astronomy, Inc., under NASA contract NAS 5-26555. Special thanks to ESA for providing pre-release versions of *Gaia* DR2 over the relevant regions. Special thanks to Bill Folkner for providing his expertise and verification of the orbit fitting results.

Facility: HST(WFC3), Gaia, SOFIA

Software: astropy (The Astropy Collaboration et al. 2018), scipy (Jones et al. 2001–), emcee (Foreman-Mackey et al. 2013), Matplotlib (Hunter 2007), photutils, spiceypy

REFERENCES

- Batygin, K., Brown, M. E., & Fraser, W. C. 2011, *ApJ*, 738, 13
- Bertin, E., & Arnouts, S. 1996, *A&AS*, 117, 393
- Braga-Ribas, F., Sicardy, B., Ortiz, J. L., et al. 2014, *Nature*, 508, 72
- Brankin, R. W., Gladwell, I., Dormand, J. R., Prince, P. J., & Seward, W. L. 1989, *ACM Transactions on Mathematical Software*, 15, 31
- Conard, S. J., Azad, F., Boldt, J. D., et al. 2005, in *Proc. SPIE*, Vol. 5906, *Astrobiology and Planetary Missions*, ed. R. B. Hoover, G. V. Levin, A. Y. Rozanov, & G. R. Gladstone, 407–420
- Elliot, J. L., Dunham, E., & Mink, D. 1977, *Nature*, 267, 328
- Elliot, J. L., Dunham, E. W., Bosh, A. S., et al. 1989, *Icarus*, 77, 148
- Elliot, J. L., Kern, S. D., Clancy, K. B., et al. 2005, *AJ*, 129, 1117
- Folkner, W. M., Williams, J. G., Boggs, D. H., Park, R. S., & Kuchynka, P. 2014, *Interplanetary Network Progress Report*, 196, 1
- Foreman-Mackey, D., Hogg, D. W., Lang, D., & Goodman, J. 2013, *PASP*, 125, 306
- Fraser, W. C., Bannister, M. T., Pike, R. E., et al. 2017, *Nature Astronomy*, 1, 0088
- Gaia Collaboration, Brown, A. G. A., Vallenari, A., et al. 2016, *A&A*, 595, A2
- Greisen, E. W., Calabretta, M. R., Valdes, F. G., & Allen, S. L. 2006, *A&A*, 446, 747
- Gwyn, S. D. J. 2014, *Journal of Instrumentation*, 9, C04003
- Hunter, J. D. 2007, *Computing In Science & Engineering*, 9, 90
- Jones, E., Oliphant, T., Peterson, P., et al. 2001–, *SciPy: Open source scientific tools for Python*, , [Online; accessed 2018-05-01]. <http://www.scipy.org/>
- Krist, J. E., Hook, R. N., & Stoehr, F. 2011, in *Proc. SPIE*, Vol. 8127, *Optical Modeling and Performance Predictions V*, 81270J
- Linscott, I., Protopapa, S., Hinson, D. P., et al. 2016, in *AAS/Division for Planetary Sciences Meeting Abstracts*, Vol. 48, *AAS/Division for Planetary Sciences Meeting Abstracts #48*, 213.04
- Michalik, D., Lindegren, L., & Hobbs, D. 2015, *A&A*, 574, A115
- Nelder, J. A., & Mead, R. 1965, *The Computer Journal*, 7, 308
- Noll, K. S., Grundy, W. M., Chiang, E. I., Margot, J.-L., & Kern, S. D. 2008, *Binaries in the Kuiper Belt*, ed. M. A. Barucci, H. Boehnhardt, D. P. Cruikshank, A. Morbidelli, & R. Dotson, 345–363
- Ortiz, J. L., Santos-Sanz, P., Sicardy, B., et al. 2017, *Nature*, 550, 219
- Petit, J.-M., Kavelaars, J. J., Gladman, B. J., et al. 2011, *AJ*, 142, 131
- Porter, S. B., Spencer, J. R., Benecchi, S., et al. 2016, *ApJL*, 828, L15
- Silverman, B. W. 1986, *Density estimation for statistics and data analysis*
- Stern, S. A., Bagenal, F., Ennico, K., et al. 2015, *Science*, 350, aad1815
- Tchebychev, P. L. 1853, *Théorie des mécanismes connus sous le nom de parallélogrammes* (Imprimerie de l'Académie impériale des sciences)
- The Astropy Collaboration, Price-Whelan, A. M., Sipőcz, B. M., et al. 2018, *ArXiv e-prints*, arXiv:1801.02634
- Volk, K., & Malhotra, R. 2017, *AJ*, 154, 62

APPENDIX

Table 3. HST/WFC3 astrometry for MU₆₉.

WFC3 Dataset	UTC Time	RA	Dec	σ RA (mas)	σ Dec (mas)
icii11r7q	2014-06-26T08:51:42.4042	18 ^h 45 ^m 10 ^s 67179	-20°53'03"0565	6.496	5.874
icii11r8q	2014-06-26T09:00:33.4117	18 ^h 45 ^m 10 ^s 63684	-20°53'03"1070	8.280	8.519
icii11raq	2014-06-26T09:09:24.4036	18 ^h 45 ^m 10 ^s 59521	-20°53'03"1753	9.150	9.504
icii11req	2014-06-26T09:18:15.3964	18 ^h 45 ^m 10 ^s 55800	-20°53'03"2431	7.130	6.348
icii11req	2014-06-26T09:27:06.4048	18 ^h 45 ^m 10 ^s 52223	-20°53'03"3121	6.935	5.378
icii12rpq	2014-06-26T12:02:50.4041	18 ^h 45 ^m 10 ^s 01995	-20°53'03"7671	5.202	5.230
icii12rqq	2014-06-26T12:11:41.4124	18 ^h 45 ^m 09 ^s 98343	-20°53'03"8268	5.274	6.928
icii12rsq	2014-06-26T12:20:32.4044	18 ^h 45 ^m 09 ^s 94411	-20°53'03"8733	8.544	8.013
icii12ruq	2014-06-26T12:29:23.3963	18 ^h 45 ^m 09 ^s 90568	-20°53'03"9530	7.870	7.667
icii12rwq	2014-06-26T12:38:14.4046	18 ^h 45 ^m 09 ^s 87100	-20°53'04"0172	10.727	11.309
iciig7cwq	2014-08-02T13:05:20.4622	18 ^h 42 ^m 15 ^s 46771	-20°56'43"2187	8.676	9.408
iciig7cyq	2014-08-02T13:14:11.4541	18 ^h 42 ^m 15 ^s 43399	-20°56'43"2084	8.216	8.844
iciig7d0q	2014-08-02T13:23:02.4624	18 ^h 42 ^m 15 ^s 40181	-20°56'43"1822	6.487	6.519
iciig7d2q	2014-08-02T13:31:53.4699	18 ^h 42 ^m 15 ^s 37313	-20°56'43"1570	9.745	7.306
iciig8kaq	2014-08-03T17:45:21.4709	18 ^h 42 ^m 10 ^s 58094	-20°56'50"4392	6.943	5.157
iciig8kcq	2014-08-03T17:54:12.4620	18 ^h 42 ^m 10 ^s 54825	-20°56'50"4185	7.896	8.639
iciig8keq	2014-08-03T18:03:03.4540	18 ^h 42 ^m 10 ^s 51593	-20°56'50"3898	8.294	12.064
iciig9rvq	2014-08-21T07:39:21.5326	18 ^h 41 ^m 08 ^s 70535	-20°58'32"3648	10.552	10.039
iciig9rwq	2014-08-21T07:48:12.5236	18 ^h 41 ^m 08 ^s 68016	-20°58'32"4070	8.175	5.865
iciig9ryq	2014-08-21T07:57:03.5164	18 ^h 41 ^m 08 ^s 65466	-20°58'32"5227	9.206	9.342
iciig9s0q	2014-08-21T08:05:54.5239	18 ^h 41 ^m 08 ^s 62880	-20°58'32"5833	8.610	8.553
iciig9s2q	2014-08-21T08:14:45.5323	18 ^h 41 ^m 08 ^s 60632	-20°58'32"6306	7.169	8.753
iciih0s4q	2014-08-21T09:14:54.5242	18 ^h 41 ^m 08 ^s 51133	-20°58'32"7412	9.255	8.626
iciih0s5q	2014-08-21T09:23:45.5317	18 ^h 41 ^m 08 ^s 48692	-20°58'32"8053	10.174	7.858
iciih0s7q	2014-08-21T09:32:36.5245	18 ^h 41 ^m 08 ^s 46256	-20°58'32"8851	11.097	6.604
iciih0s9q	2014-08-21T09:41:27.5164	18 ^h 41 ^m 08 ^s 43633	-20°58'32"9342	7.150	7.405

Table 3 continued

Table 3 (*continued*)

WFC3				σ RA	σ Dec
Dataset	UTC Time	RA	Dec	(mas)	(mas)
iciih0sbq	2014-08-21T09:50:18.5248	18 ^h 41 ^m 08 ^s 41206	-20°58'33"0122	6.504	7.669
iciih3byq	2014-08-23T04:14:48.5240	18 ^h 41 ^m 03 ^s 42093	-20°58'42"4838	8.822	8.230
iciih3bzq	2014-08-23T04:23:39.5160	18 ^h 41 ^m 03 ^s 39764	-20°58'42"5345	8.260	7.247
iciih3c1q	2014-08-23T04:32:30.5243	18 ^h 41 ^m 03 ^s 37316	-20°58'42"6359	8.590	8.633
iciih3c3q	2014-08-23T04:41:21.5318	18 ^h 41 ^m 03 ^s 34782	-20°58'42"7163	12.208	8.579
iciih3c5q	2014-08-23T04:50:12.5401	18 ^h 41 ^m 03 ^s 32417	-20°58'42"7810	8.243	8.709
iciih4c7q	2014-08-23T05:50:22.5239	18 ^h 41 ^m 03 ^s 23676	-20°58'42"8412	7.167	7.342
iciih4c8q	2014-08-23T05:59:13.5323	18 ^h 41 ^m 03 ^s 21355	-20°58'42"8952	7.158	5.986
iciih4caq	2014-08-23T06:08:04.5242	18 ^h 41 ^m 03 ^s 18844	-20°58'42"9833	8.322	7.320
iciih4ccq	2014-08-23T06:16:55.5162	18 ^h 41 ^m 03 ^s 16358	-20°58'43"0496	8.754	10.610
iciih4ceq	2014-08-23T06:25:46.5236	18 ^h 41 ^m 03 ^s 14306	-20°58'43"1152	8.151	7.563
icij5ydq	2014-10-15T01:36:27.6413	18 ^h 40 ^m 43 ^s 94965	-21°01'45"5109	9.931	10.104
icij5yfq	2014-10-15T01:45:18.6488	18 ^h 40 ^m 43 ^s 95600	-21°01'45"5515	11.179	10.119
icij5yhq	2014-10-15T01:54:09.6572	18 ^h 40 ^m 43 ^s 96306	-21°01'45"5758	9.929	8.851
icij5yjq	2014-10-15T02:03:00.6655	18 ^h 40 ^m 43 ^s 96693	-21°01'45"6258	8.356	8.839
icij5yoq	2014-10-15T02:11:51.6410	18 ^h 40 ^m 43 ^s 97731	-21°01'45"6487	7.518	7.322
icij6yyq	2014-10-15T03:29:42.6497	18 ^h 40 ^m 44 ^s 10758	-21°01'45"6562	9.126	10.111
icij6z2q	2014-10-15T03:47:24.6647	18 ^h 40 ^m 44 ^s 12125	-21°01'45"7481	6.790	6.469
icij7etq	2014-10-16T04:40:32.6328	18 ^h 40 ^m 46 ^s 48368	-21°01'46"5691	11.437	8.316
icij7eyq	2014-10-16T05:07:05.6570	18 ^h 40 ^m 46 ^s 50539	-21°01'46"7101	8.268	8.288
icij9c6q	2014-10-22T08:44:42.6722	18 ^h 41 ^m 02 ^s 50094	-21°01'49"7408	9.897	11.963
icij9c7q	2014-10-22T08:53:33.6805	18 ^h 41 ^m 02 ^s 51372	-21°01'49"8238	11.269	9.985
icij9c9q	2014-10-22T09:02:24.6733	18 ^h 41 ^m 02 ^s 52511	-21°01'49"8756	7.835	6.873
icij9cdq	2014-10-22T09:20:06.6727	18 ^h 41 ^m 02 ^s 54616	-21°01'49"9420	11.968	9.530
ict101egq	2015-05-04T16:36:10.0607	18 ^h 54 ^m 04 ^s 85674	-20°45'17"1327	8.464	8.629
ict101eiq	2015-05-04T16:44:59.0697	18 ^h 54 ^m 04 ^s 83515	-20°45'17"0929	8.467	7.449
ict101ekq	2015-05-04T16:53:48.0771	18 ^h 54 ^m 04 ^s 81533	-20°45'17"0358	8.416	8.155
ict101emq	2015-05-04T17:02:37.0688	18 ^h 54 ^m 04 ^s 79577	-20°45'16"9791	8.591	7.354
ict103vvq	2015-07-04T14:30:23.1969	18 ^h 50 ^m 04 ^s 47370	-20°49'11"5823	8.552	11.691
ict103vwq	2015-07-04T14:39:13.1961	18 ^h 50 ^m 04 ^s 43802	-20°49'11"6027	7.657	7.162

Table 3 continued

Table 3 (*continued*)

WFC3				σ RA	σ Dec
Dataset	UTC Time	RA	Dec	(mas)	(mas)
ict103vyq	2015-07-04T14:48:03.1962	18 ^h 50 ^m 04 ^s 39866	-20°49'11"6196	8.622	8.340
ict103w0q	2015-07-04T14:56:53.1963	18 ^h 50 ^m 04 ^s 36010	-20°49'11"6368	5.515	6.545
ict103w2q	2015-07-04T15:05:43.1963	18 ^h 50 ^m 04 ^s 32408	-20°49'11"6547	5.728	6.567
id3m01hhq	2016-03-15T00:11:56.2344	18 ^h 59 ^m 12 ^s 34397	-20°42'13"6731	10.700	8.556
id3m01hiq	2016-03-15T00:20:44.2342	18 ^h 59 ^m 12 ^s 35540	-20°42'13"6779	11.293	10.247
id3m01hlq	2016-03-15T00:29:32.2350	18 ^h 59 ^m 12 ^s 36343	-20°42'13"6355	9.891	10.908
id3m01hqq	2016-03-15T00:38:20.2349	18 ^h 59 ^m 12 ^s 37280	-20°42'13"5403	8.836	7.947
id3m01hsq	2016-03-15T00:47:08.2340	18 ^h 59 ^m 12 ^s 38636	-20°42'13"4204	10.946	10.261
id3m02soq	2016-05-15T02:19:56.3589	18 ^h 59 ^m 07 ^s 54093	-20°39'50"5456	6.365	6.087
id5901eqq	2016-07-25T16:49:31.5321	18 ^h 53 ^m 53 ^s 03748	-20°46'32"2179	9.215	10.954
id5901erq	2016-07-25T16:58:19.5485	18 ^h 53 ^m 53 ^s 00295	-20°46'32"2817	7.198	6.205
id5901etq	2016-07-25T17:07:07.5328	18 ^h 53 ^m 52 ^s 96820	-20°46'32"3433	12.890	10.688
id5901evq	2016-07-25T17:15:55.5491	18 ^h 53 ^m 52 ^s 93097	-20°46'32"3865	7.764	6.118
id5901exq	2016-07-25T17:24:43.5490	18 ^h 53 ^m 52 ^s 89789	-20°46'32"4503	11.000	11.074
id5902a9q	2016-10-21T05:07:24.7290	18 ^h 51 ^m 48 ^s 31696	-20°53'07"6653	9.090	9.960
id5902adq	2016-10-21T05:25:00.7297	18 ^h 51 ^m 48 ^s 33435	-20°53'07"5531	10.424	8.911
id5902afq	2016-10-21T05:33:48.7295	18 ^h 51 ^m 48 ^s 34571	-20°53'07"4620	8.163	8.154
id5953gxq	2017-05-01T21:02:43.4730	19 ^h 05 ^m 08 ^s 03529	-20°33'13"4643	5.497	5.760
id5953gyq	2017-05-01T21:11:31.4574	19 ^h 05 ^m 08 ^s 02054	-20°33'13"4987	6.192	5.165
id5953h0q	2017-05-01T21:20:19.4738	19 ^h 05 ^m 08 ^s 00391	-20°33'13"5663	6.838	5.995
id5953h2q	2017-05-01T21:29:07.4736	19 ^h 05 ^m 07 ^s 98675	-20°33'13"6156	7.427	7.120
id5953h4q	2017-05-01T21:37:55.4744	19 ^h 05 ^m 07 ^s 96987	-20°33'13"6559	9.199	9.665
id5904wiq	2017-05-25T17:27:55.5436	19 ^h 04 ^m 06 ^s 07475	-20°34'02"9420	6.379	5.984
id5904wkq	2017-05-25T17:36:43.5280	19 ^h 04 ^m 06 ^s 04412	-20°34'02"9634	6.826	5.843
id5904wmq	2017-05-25T17:45:31.5434	19 ^h 04 ^m 06 ^s 01468	-20°34'02"9165	6.391	7.571
id8i01skq	2017-06-25T07:37:23.6242	19 ^h 01 ^m 55 ^s 18310	-20°36'53"1436	6.396	6.501
id8i01slq	2017-06-25T07:46:11.6241	19 ^h 01 ^m 55 ^s 14905	-20°36'53"2328	6.156	6.246
id8i01snq	2017-06-25T07:54:59.6240	19 ^h 01 ^m 55 ^s 11119	-20°36'53"3237	8.370	7.069
id8i01spq	2017-06-25T08:03:47.6231	19 ^h 01 ^m 55 ^s 07326	-20°36'53"4114	9.158	7.480
id8i01srq	2017-06-25T08:12:35.6074	19 ^h 01 ^m 55 ^s 03946	-20°36'53"4787	5.086	6.422

Table 3 continued

Table 3 (*continued*)

WFC3				σ RA	σ Dec
Dataset	UTC Time	RA	Dec	(mas)	(mas)
id8i02stq	2017-06-25T09:12:44.6149	19 ^h 01 ^m 54 ^s 86318	-20°36'53"5963	9.097	7.171
id8i02suq	2017-06-25T09:21:32.6148	19 ^h 01 ^m 54 ^s 82820	-20°36'53"6883	7.471	5.608
id8i02swq	2017-06-25T09:30:20.6156	19 ^h 01 ^m 54 ^s 79110	-20°36'53"7914	4.644	4.964
id8i02syq	2017-06-25T09:39:08.6155	19 ^h 01 ^m 54 ^s 75385	-20°36'53"8649	6.545	5.584
id8i02t0q	2017-06-25T09:47:56.6163	19 ^h 01 ^m 54 ^s 71922	-20°36'53"9495	5.128	4.908
id8i03t4q	2017-06-25T10:48:05.6073	19 ^h 01 ^m 54 ^s 54329	-20°36'54"0349	6.562	7.028
id8i03t7q	2017-06-25T10:56:53.6081	19 ^h 01 ^m 54 ^s 50911	-20°36'54"1633	5.107	5.347
id8i03t9q	2017-06-25T11:05:41.6080	19 ^h 01 ^m 54 ^s 47159	-20°36'54"2478	5.968	7.687
id8i03tbq	2017-06-25T11:14:29.6070	19 ^h 01 ^m 54 ^s 43409	-20°36'54"3285	5.276	5.845
id8i04tfq	2017-06-25T12:23:27.6227	19 ^h 01 ^m 54 ^s 22363	-20°36'54"5187	5.490	6.343
id8i04tgq	2017-06-25T12:32:15.6071	19 ^h 01 ^m 54 ^s 18806	-20°36'54"6009	8.028	7.617
id8i04tiq	2017-06-25T12:41:03.6234	19 ^h 01 ^m 54 ^s 15199	-20°36'54"7131	5.463	6.314
id8i04tkq	2017-06-25T12:49:51.6242	19 ^h 01 ^m 54 ^s 11435	-20°36'54"7939	6.269	6.610
id8i04tmq	2017-06-25T12:58:39.6240	19 ^h 01 ^m 54 ^s 07993	-20°36'54"8631	5.614	5.066
id8i05txq	2017-06-25T15:34:10.6003	19 ^h 01 ^m 53 ^s 58450	-20°36'55"4388	5.972	6.391
id8i05tyq	2017-06-25T15:42:58.5993	19 ^h 01 ^m 53 ^s 54976	-20°36'55"5321	6.780	5.843
id8i05u0q	2017-06-25T15:51:46.6156	19 ^h 01 ^m 53 ^s 51243	-20°36'55"6468	5.993	6.287
id8i05u2q	2017-06-25T16:00:34.5991	19 ^h 01 ^m 53 ^s 47352	-20°36'55"7304	8.008	7.278
id8i05u4q	2017-06-25T16:09:22.5999	19 ^h 01 ^m 53 ^s 43916	-20°36'55"7992	7.822	8.149
id8i06u6q	2017-06-25T17:09:30.6155	19 ^h 01 ^m 53 ^s 26390	-20°36'55"9206	8.896	9.491
id8i06u7q	2017-06-25T17:18:18.5998	19 ^h 01 ^m 53 ^s 23041	-20°36'55"9925	7.080	6.282
id8i06u9q	2017-06-25T17:27:06.5989	19 ^h 01 ^m 53 ^s 19192	-20°36'56"1086	8.232	6.485
id8i06ubq	2017-06-25T17:35:54.6152	19 ^h 01 ^m 53 ^s 15377	-20°36'56"2064	8.378	7.502
id8i06udq	2017-06-25T17:44:42.5987	19 ^h 01 ^m 53 ^s 11963	-20°36'56"2669	8.389	7.610
id8i07crq	2017-06-26T07:27:41.6079	19 ^h 01 ^m 50 ^s 38003	-20°37'00"1011	6.654	7.075
id8i07ctq	2017-06-26T07:36:29.6078	19 ^h 01 ^m 50 ^s 34397	-20°37'00"1993	8.378	7.315
id8i07cwq	2017-06-26T07:45:17.6068	19 ^h 01 ^m 50 ^s 30856	-20°37'00"3029	5.666	6.112
id8i07cyq	2017-06-26T07:54:05.6068	19 ^h 01 ^m 50 ^s 27096	-20°37'00"4163	5.126	6.084
id8i07d1q	2017-06-26T08:02:53.6066	19 ^h 01 ^m 50 ^s 23531	-20°37'00"4803	5.526	5.040
id8i08daq	2017-06-26T09:03:03.6233	19 ^h 01 ^m 50 ^s 05904	-20°37'00"5910	10.279	6.816

Table 3 continued

Table 3 (*continued*)

WFC3				σ RA	σ Dec
Dataset	UTC Time	RA	Dec	(mas)	(mas)
id8i08dbq	2017-06-26T09:11:51.6232	19 ^h 01 ^m 50 ^s 02460	-20°37'00"6563	6.995	6.221
id8i08ddq	2017-06-26T09:20:39.6240	19 ^h 01 ^m 49 ^s 98730	-20°37'00"7742	5.442	6.276
id8i08dfq	2017-06-26T09:29:27.6238	19 ^h 01 ^m 49 ^s 94929	-20°37'00"8552	8.475	8.027
id8i08diq	2017-06-26T09:38:15.6229	19 ^h 01 ^m 49 ^s 91336	-20°37'00"9372	5.958	5.866
id8i09dkq	2017-06-26T10:38:25.6075	19 ^h 01 ^m 49 ^s 73909	-20°37'01"0586	5.690	6.374
id8i09dlq	2017-06-26T10:47:13.6075	19 ^h 01 ^m 49 ^s 70415	-20°37'01"1403	5.856	7.255
id8i09dnq	2017-06-26T10:56:01.6083	19 ^h 01 ^m 49 ^s 66535	-20°37'01"2596	6.223	5.913
id8i09dpq	2017-06-26T11:04:49.6081	19 ^h 01 ^m 49 ^s 62903	-20°37'01"3395	6.642	8.355
id8i10dtq	2017-06-26T12:13:46.6155	19 ^h 01 ^m 49 ^s 41640	-20°37'01"5098	6.808	7.171
id8i10duq	2017-06-26T12:22:34.5990	19 ^h 01 ^m 49 ^s 38307	-20°37'01"6174	5.280	6.514
id8i10dwq	2017-06-26T12:31:22.5989	19 ^h 01 ^m 49 ^s 34460	-20°37'01"7232	6.411	6.077
id8i10dyq	2017-06-26T12:40:10.5997	19 ^h 01 ^m 49 ^s 30648	-20°37'01"8035	4.767	5.779
id8i10e0q	2017-06-26T12:48:58.5996	19 ^h 01 ^m 49 ^s 27112	-20°37'01"8889	5.476	5.328
id8i11eiq	2017-06-26T17:00:38.6153	19 ^h 01 ^m 48 ^s 45153	-20°37'02"9441	8.482	8.030
id8i11ejq	2017-06-26T17:09:26.5988	19 ^h 01 ^m 48 ^s 41519	-20°37'03"0318	8.076	7.328
id8i11elq	2017-06-26T17:18:14.5987	19 ^h 01 ^m 48 ^s 37703	-20°37'03"1593	6.787	9.734
id8i11eoq	2017-06-26T17:27:02.5995	19 ^h 01 ^m 48 ^s 33962	-20°37'03"2174	7.868	10.419
id8i11eqq	2017-06-26T17:35:50.5993	19 ^h 01 ^m 48 ^s 30633	-20°37'03"2853	5.290	4.749
id8i12esq	2017-06-26T18:40:22.5998	19 ^h 01 ^m 48 ^s 11203	-20°37'03"4625	6.732	5.483
id8i12etq	2017-06-26T18:49:10.5997	19 ^h 01 ^m 48 ^s 07483	-20°37'03"5526	7.972	8.115
id8i12evq	2017-06-26T18:57:58.6152	19 ^h 01 ^m 48 ^s 03824	-20°37'03"6610	8.285	6.559
id8i12exq	2017-06-26T19:06:46.5987	19 ^h 01 ^m 48 ^s 00234	-20°37'03"7452	6.643	8.809
id8i13lvq	2017-06-28T05:32:56.6157	19 ^h 01 ^m 41 ^s 04678	-20°37'13"8017	6.423	5.150
id8i13lwq	2017-06-28T05:41:44.6156	19 ^h 01 ^m 41 ^s 01136	-20°37'13"9082	5.077	4.970
id8i13lyq	2017-06-28T05:50:32.6155	19 ^h 01 ^m 40 ^s 97517	-20°37'14"0037	4.861	4.601
id8i13m0q	2017-06-28T05:59:20.6163	19 ^h 01 ^m 40 ^s 93805	-20°37'14"1005	6.567	6.656
id8i13m3q	2017-06-28T06:08:08.6161	19 ^h 01 ^m 40 ^s 90205	-20°37'14"1767	6.510	5.490
id8i14m5q	2017-06-28T07:08:17.6081	19 ^h 01 ^m 40 ^s 72466	-20°37'14"2761	4.571	4.725
id8i14m6q	2017-06-28T07:17:05.6071	19 ^h 01 ^m 40 ^s 68925	-20°37'14"3838	5.149	5.421
id8i14m8q	2017-06-28T07:25:53.6070	19 ^h 01 ^m 40 ^s 65300	-20°37'14"4841	6.629	6.663

Table 3 continued

Table 3 (*continued*)

WFC3				σ RA	σ Dec
Dataset	UTC Time	RA	Dec	(mas)	(mas)
id8i14maq	2017-06-28T07:34:41.6069	19 ^h 01 ^m 40 ^s 61368	-20°37'14"6007	5.686	6.738
id8i14mcq	2017-06-28T07:43:29.6077	19 ^h 01 ^m 40 ^s 58000	-20°37'14"6548	9.290	7.692
id8i15meq	2017-06-28T08:43:37.6078	19 ^h 01 ^m 40 ^s 40122	-20°37'14"7501	6.204	5.847
id8i15mfq	2017-06-28T08:52:25.6076	19 ^h 01 ^m 40 ^s 36750	-20°37'14"8581	6.689	5.987
id8i15mhq	2017-06-28T09:01:13.6067	19 ^h 01 ^m 40 ^s 33020	-20°37'14"9650	4.155	4.586
id8i15mjg	2017-06-28T09:10:01.6075	19 ^h 01 ^m 40 ^s 29244	-20°37'15"0795	5.379	6.786
id8i15mlq	2017-06-28T09:18:49.6082	19 ^h 01 ^m 40 ^s 25699	-20°37'15"1355	5.312	5.183
id8i16mnq	2017-06-28T10:18:59.6232	19 ^h 01 ^m 40 ^s 07761	-20°37'15"2312	8.361	9.052
id8i16moq	2017-06-28T10:27:47.6230	19 ^h 01 ^m 40 ^s 04398	-20°37'15"3414	5.624	5.232
id8i16mqg	2017-06-28T10:36:35.6238	19 ^h 01 ^m 40 ^s 00812	-20°37'15"4442	5.787	5.530
id8i16msq	2017-06-28T10:45:23.6237	19 ^h 01 ^m 39 ^s 96933	-20°37'15"5235	7.036	6.210
id8i16muq	2017-06-28T10:54:11.6236	19 ^h 01 ^m 39 ^s 93349	-20°37'15"6005	6.019	6.975
id8i17obq	2017-06-28T15:05:02.6151	19 ^h 01 ^m 39 ^s 10997	-20°37'16"6579	7.323	5.389
id8i17ocq	2017-06-28T15:13:50.6003	19 ^h 01 ^m 39 ^s 07618	-20°37'16"7759	4.671	4.676
id8i17oeq	2017-06-28T15:22:38.6002	19 ^h 01 ^m 39 ^s 03924	-20°37'16"8792	6.235	6.510
id8i17ogq	2017-06-28T15:31:26.6157	19 ^h 01 ^m 39 ^s 00035	-20°37'16"9833	6.294	7.602
id8i17oiq	2017-06-28T15:40:14.5992	19 ^h 01 ^m 38 ^s 96504	-20°37'17"0334	5.759	4.966
id8i18olq	2017-06-28T16:49:11.6238	19 ^h 01 ^m 38 ^s 75129	-20°37'17"2404	6.936	5.735
id8i18onq	2017-06-28T16:57:59.6237	19 ^h 01 ^m 38 ^s 71440	-20°37'17"3650	6.058	5.273
id8i18opq	2017-06-28T17:06:47.6228	19 ^h 01 ^m 38 ^s 67779	-20°37'17"4586	5.509	5.146
id8i18orq	2017-06-28T17:15:35.6071	19 ^h 01 ^m 38 ^s 64165	-20°37'17"5070	6.706	5.493
id8i19geq	2017-07-04T04:34:39.6076	19 ^h 01 ^m 11 ^s 82432	-20°37'57"6469	6.321	8.507
id8i19gfq	2017-07-04T04:43:27.6239	19 ^h 01 ^m 11 ^s 79038	-20°37'57"7960	7.592	8.341
id8i19gpq	2017-07-04T04:52:15.6074	19 ^h 01 ^m 11 ^s 75312	-20°37'57"9103	6.640	7.705
id8i19grq	2017-07-04T05:01:03.6229	19 ^h 01 ^m 11 ^s 71403	-20°37'57"9920	9.998	5.635
id8i19gtq	2017-07-04T05:09:51.6228	19 ^h 01 ^m 11 ^s 67763	-20°37'58"0126	9.165	7.546
id8i20h2q	2017-07-04T06:10:00.6147	19 ^h 01 ^m 11 ^s 49739	-20°37'58"1574	7.833	7.575
id8i20h3q	2017-07-04T06:18:48.6155	19 ^h 01 ^m 11 ^s 46445	-20°37'58"2853	6.418	5.336
id8i20h5q	2017-07-04T06:27:36.6154	19 ^h 01 ^m 11 ^s 42716	-20°37'58"4153	5.600	5.271
id8i20h7q	2017-07-04T06:36:24.6153	19 ^h 01 ^m 11 ^s 38824	-20°37'58"4798	6.678	7.588

Table 3 continued